

A microscopic approach to study the onset of a highly infectious disease spreading

Krithika Rathinakumar* and Annalisa Quaini*

*Department of Mathematics, University of Houston, 3551 Cullen Blvd, Houston TX 77204

krithika.trk@gmail.com; quaini@math.uh.edu

February 1, 2022

Abstract

We combine a pedestrian dynamics model with a contact tracing method to simulate the initial spreading of a highly infectious airborne disease in a confined environment. We focus on a medium size population (up to 1000 people) with a small number of infectious people (1 or 2) and the rest of the people is divided between immune and susceptible. We adopt a space-continuous model that represents pedestrian dynamics by the forces acting on them, i.e. a microscopic force-based model. Once discretized, the model results in a high-dimensional system of second order ordinary differential equations. Before adding the contact tracing to the pedestrian dynamics model, we calibrate the model parameters, validate the model against empirical data, and show that pedestrian self-organization into lanes can be captured. We consider an explicit approach for contact tracing by introducing a sickness domain around a sick person. A healthy but susceptible person who remains in the sickness domain for a certain amount of time may get infected (with a prescribed probability) and become a so-called secondary contact. As a concrete setting to simulate the onset of disease spreading, we consider terminals in two US airports: Hobby Airport in Houston and the Atlanta International Airport. We consider different scenarios and we quantify the increase in average number of secondary contacts increases as a given terminal becomes more densely populated, the percentage of immune people decreases, the number of primary contacts increases, and areas of high density (such as the boarding buses) are present.

Keywords: Crowd dynamics, contact tracing, disease spreading, complex systems

1 Introduction

The focus of this work is to study the initiation of disease spreading in a confined, yet complex environment (e.g. an airport terminal), and in a medium size population (up to 1000 people) with a small number of infectious people (1 or 2). Standard epidemic theory models describe the

evolution of disease spreading in terms of groups that are susceptible to, infected with and recovered from a particular disease. The SIR (Susceptible Infected Recovered - see, e.g., [28, 45]) and SIS (Susceptible Infected Susceptible - see, e.g., [24, 18]) models are the foundation of almost all of mathematical epidemiology. To quantify the transmission dynamics through contact with healthy individuals, these models use the basic reproduction number, which measures the number of infected people (secondary contacts) from an infectious person (primary contact) in a population where all the people are susceptible. Most models predicting the severity of an epidemic estimate the basic reproduction number for large population sizes. See, e.g., [12, 31, 26] and references therein. Such models are typically not valid when the number of infected individuals is small and the size of healthy population is medium. Medium sized population are typical of confined environments like airports and hospital waiting rooms, which are the most likely transmittal places during the initial stage of disease spreading. See, e.g., [37, 38] Understanding contact tracing associated with such environments is of paramount importance for an early suppression of an epidemic.

We propose a simple approach for contact tracing built on a microscopic pedestrian dynamics model. Usually, contact tracing is meant as a disease control strategy in which the people who have been in close contact to infectious persons are traced. These traced people are monitored so that if they become symptomatic they can be efficiently isolated and the disease transmission can be contained [16, 17]. The effectiveness of contact tracing as a control strategy for ebola and tuberculosis have been studied theoretically in, e.g., [44, 19]. Previous works on contact tracing use a wide range of methodologies from individual based models on specific networks to compartmental ordinary differential equations at the population level. See, e.g., [41, 30, 31, 2, 12] and references therein. Many differential equation models incorporate contact tracing implicitly (see, e.g. [40, 44]). In our simulations, contact tracing is limited to pedestrians coming in contact during a short time span (up to 1 hour). The contact tracing method is combined with a pedestrian dynamics model to estimate the number of people that could potentially be infected by a few sick people around them, thereby providing a tool to study the onset of disease spreading.

A very large variety of models have been developed over the years to describe the complex dynamical behavior of pedestrian crowds. The different mathematical models can be divided into three main categories depending on the (macroscopic, mesoscopic, microscopic) scale of observation [8]. Macroscopic models (see, e.g., [25, 48]) are suitable for high density, large-scale systems. Thus, they will not be considered for the proposed work. The mesoscale approach [5, 1, 4, 7, 6, 9, 10, 6, 11, 3, 29] derives a Boltzmann-type evolution equation for the statistical distribution function of the position and velocity of the pedestrians, in a framework close to that of the kinetic theory of gases. Microscopic force-based models, which use Newtonian mechanics to interpret pedestrian movement as the physical interaction between the people and the environment, are one of the most popular modeling paradigms of continuous models because they describe the movement of pedestrians well qualitatively. See, e.g., [20, 22, 23, 50, 39, 14, 55, 33] and references therein. Collective phenomena, like unidirectional or bidirectional flow in a corridor [35, 49, 52], lane formation [22, 21, 53], oscillations at bottlenecks [22, 21], the faster-is-slower effect [32, 42], emergency evacuation from buildings [21, 53, 34], are well reproduced. Other advantages of these methods are the ease of

implementation, and in particular parallel implementation, and the fact that they permit higher resolution for geometry and time. Because of these advantages, we choose to build our contact tracing method on a microscopic force-based model first presented in [15].

In most of the references cited above, models have been shown to replicate various cases of pedestrian movement qualitatively through analysis and/or numerical simulations. The *quantitative* validation of pedestrian flow models is complicated by the lack of reliable experimental data. In addition, the few available datasets show large differences [46, 47, 54]. After a calibration of the model parameters, we validate the model in [15] by comparing with empirical data from [54]. We obtain a good quantitative agreement between the computed and measured fundamental diagrams for a set of 9 experiments, all involving unidirectional motion in a corridor. We run a series of tests to understand self-organized lane formation, as this is relevant to the kind of environment we focus on. Finally, we mention that adjustment of the parameters and data assimilations have also been proposed in [51, 27] to make evolutionary models more reliable.

The validated pedestrian dynamics model is then combined with a simple method to trace contact. One or two sick people, referred to as primary contacts, are introduced in the pedestrian population. The people infected by the primary contact are called secondary contacts. We consider an explicit approach for contact tracing by introducing a sickness domain around a primary contact. A healthy but susceptible person who remains in that sickness domain for a certain amount of time may get infected (with a prescribed probability) and become a secondary contact. As a concrete setting to simulate the onset of disease spreading, we consider terminals in two US airports: Hobby Airport in Houston and the Atlanta International Airport. We consider different scenarios: variable population size, variable percentage of immune (non-susceptible) population, boarding bridges or boarding buses. Through the numerical simulations, we quantify the increase in average number of secondary contacts increases as a given terminal becomes more densely populated, the percentage of immune people decreases, the number of primary contacts increases, and areas of high density (such as the boarding buses) are present.

The outline of this paper is as follows. In Sec. 2, we introduce the force-based microscopic model for pedestrian dynamics we will build upon, we describe the numerical method, calibrate the model parameters and validate the model against experimental data. In Sec. 3, we show that the model is capable of reproducing self-organization of pedestrians. In Sec. 4, we present our contact tracing method and combine it with the pedestrian dynamics model to simulate the initial spreading of a highly infectious airborne disease. We report the average number of people infected by one or two sick people in terminals of Hobby Airport and Atlanta International Airport for different scenarios. Conclusions are drawn in Sec. 5.

2 A microscopic force-based model for pedestrian dynamics

We briefly present the model we focus on, which was introduced in [15]. Let us consider a group of N pedestrians in a bounded geometry Ω . Each pedestrian is modeled as a circular disk with a

given radius. The dynamics of each pedestrian over a time interval of interest $(0, T]$ is modeled using Newton's second law, i.e. for pedestrian i with mass m_i and center of mass at \mathbf{r}_i the law of motion is:

$$m_i \ddot{\mathbf{r}}_i = \mathbf{f}_i, \quad i = 1, \dots, N, \quad (1)$$

where \mathbf{f}_i represents the total forces acting on the pedestrian. Source term \mathbf{f}_i includes the force driving the pedestrian towards their target and the repulsive forces acting on the pedestrian from other pedestrians, walls, and other obstacles. Finding an appropriate description of \mathbf{f}_i to obtain realistic pedestrian motion is not a trivial task.

Given $h > 0$, the boundary $\partial\Omega$ is represented as a set of N_b points: $\mathcal{B} = \{\mathbf{r}_k \in \partial\Omega\}_{k=0}^{N_b}$ with $\|\mathbf{r}_{k+1} - \mathbf{r}_k\| = h$, for $k = 0, \dots, N_b - 1$. The set of boundary points acting on pedestrian i at time $t \in (0, T]$ is:

$$\mathcal{B}_i = \{j \in \mathbb{N}, j \leq N_b : \mathbf{r}_j \in \mathcal{B} \text{ and } \|\mathbf{r}_j - \mathbf{r}_i\| \leq r_w\},$$

where $\|\cdot\|$ denotes the Euclidean norm in \mathbb{R}^2 and r_w is a cutoff radius for pedestrian-wall interaction. The set of all pedestrians that influence the motion of pedestrian i at a certain time is:

$$\mathcal{P}_i = \{j \in \mathbb{N}, j \leq N : \|\mathbf{r}_j - \mathbf{r}_i\| \leq r_p\},$$

where r_p is a cutoff radius for pedestrian-pedestrian interaction. We assume that the total forces \mathbf{f}_i consist of three contributions:

$$\mathbf{f}_i = \mathbf{f}_i^{tar} + \sum_{j \in \mathcal{P}_i} \mathbf{f}_{ij}^{ped} + \sum_{j \in \mathcal{B}_i} \mathbf{f}_{ij}^{bou}, \quad i = 1, \dots, N, \quad (2)$$

where \mathbf{f}_i^{tar} is the force driving pedestrian i to their target, \mathbf{f}_{ij}^{ped} is the repulsive force pedestrian j exerts on pedestrian i , and \mathbf{f}_{ij}^{bou} is the repulsive force due to the domain boundary. Repulsive forces \mathbf{f}_{ij}^{ped} and \mathbf{f}_{ij}^{bou} model the pedestrians' attempt to avoid collisions and contact by changing their direction.

The driving force models the intention of a pedestrian to reach a destination with a certain desired speed \bar{v}_i :

$$\mathbf{f}_i^{tar} = m_i \frac{\bar{v}_i \mathbf{e}_i - \mathbf{v}_i}{\tau}, \quad (3)$$

where \mathbf{e}_i is the unit vector directed from pedestrian i to their target, $\mathbf{v}_i = \dot{\mathbf{r}}_i$ is the velocity of pedestrian i , and τ is a time constant. To represent more involved paths, we generate a sequence of "checkpoints" along the path and for each checkpoint j we specify a radius r_j . Checkpoint j is considered to be reached when the pedestrian is within a distance r_j of it. Once a path is assigned to a pedestrian, the target is the first checkpoint along the path and when the first checkpoint is reached the target is updated to the second checkpoint, and so on.

In order to define repulsive force \mathbf{f}_{ij}^{ped} in (2), we need to introduce some notation. The vector connecting pedestrian i with pedestrian j , directed from i to j , and the corresponding unit vector are denoted by:

$$\mathbf{r}_{ij} = \mathbf{r}_j - \mathbf{r}_i, \quad \mathbf{e}_{ij} = \frac{\mathbf{r}_{ij}}{\|\mathbf{r}_{ij}\|}.$$

We assume that pedestrian i has an effective diameter d_i that depends linearly on their velocity:

$$d_i(\mathbf{v}_i) = d_i^0 + \tau_d \|\mathbf{v}_i\|, \quad (4)$$

d_i^0 being their diameter at rest and τ_d being a proportionality parameter. Eq. (4) accounts for the fact that a faster pedestrian has an effective larger diameter since he/she will keep obstacles and other pedestrians at a larger distance. The effective distance between pedestrians i and j is then:

$$d_{ij} = \|\mathbf{r}_{ij}\| - \frac{1}{2}(d_i(\mathbf{v}_i) + d_j(\mathbf{v}_j)). \quad (5)$$

We can now write the repulsive force as:

$$\mathbf{f}_{ij}^{ped} = -m_i k_{ij} \frac{(\mu \bar{v}_i + v_{ij})^2}{d_{ij}} \mathbf{e}_{ij}, \quad (6)$$

where μ is a parameter used to tune the strength of the force, v_{ij} is the component of the velocity of i relative to j in the direction of \mathbf{e}_{ij} :

$$v_{ij} = \frac{1}{2} [(\mathbf{v}_i - \mathbf{v}_j) \cdot \mathbf{e}_{ij} + |(\mathbf{v}_i - \mathbf{v}_j) \cdot \mathbf{e}_{ij}|] = \begin{cases} (\mathbf{v}_i - \mathbf{v}_j) \cdot \mathbf{e}_{ij} & \text{if } (\mathbf{v}_i - \mathbf{v}_j) \cdot \mathbf{e}_{ij} > 0, \\ 0 & \text{otherwise,} \end{cases} \quad (7)$$

and k_{ij} is a coefficient that reduces the action-field of the repulsive force to the angle of vision of each pedestrian (i.e., 180°):

$$k_{ij} = \frac{1}{2} \frac{\mathbf{v}_i \cdot \mathbf{e}_{ij} + |\mathbf{v}_i \cdot \mathbf{e}_{ij}|}{\|\mathbf{v}_i\|} = \begin{cases} \frac{\mathbf{v}_i \cdot \mathbf{e}_{ij}}{\|\mathbf{v}_i\|} & \text{if } \mathbf{v}_i \cdot \mathbf{e}_{ij} > 0 \text{ and } \|\mathbf{v}_i\| \neq 0, \\ 0 & \text{otherwise.} \end{cases} \quad (8)$$

As is intuitive, repulsive force (6) is directed in the opposite direction of \mathbf{e}_{ij} and its modulus is inversely proportional to the effective distance between pedestrians i and pedestrian j . Moreover, the strength of the repulsive force \mathbf{f}_{ij}^{ped} depends on the angle between \mathbf{v}_i and \mathbf{e}_{ij} . In fact, the coefficient k_{ij} takes its maximum value (i.e., 1) when pedestrian i is moving in the same direction as \mathbf{e}_{ij} and it takes its minimum value (i.e., 0) when the angle between \mathbf{v}_i and \mathbf{e}_{ij} is bigger than 90° . Notice that, thanks to the definition of v_{ij} , pedestrian i feels the repulsive force due to pedestrian j only if they are moving toward each other. So, e.g., if pedestrian j is close to pedestrian i , but faster than and ahead of i , then $\mathbf{f}_{ij}^{ped} = \mathbf{0}$. The term $\mu \bar{v}_i$ at the numerator in eq. (6) prevents collisions

when the distance between the two pedestrian is small and the relative speed is low, which would lead to an otherwise small repulsive force. The case $\mu = 0$ corresponds to the centrifugal force model introduced in [53], which is known to lead to realistic results only if supplemented with a collision detection technique. See also [13] for details.

In order to define \mathbf{f}_{ij}^{bou} , we note that the repulsive force between a pedestrian i and a wall is zero if i is walking parallel to the wall. In the model though, this is not enough to avoid very small repulsive forces when the pedestrians walks almost parallel to the wall. For this reason, we assume that each pedestrian i feels the repulsive action of three points lying on the boundary: the closest boundary point to pedestrian i denoted by \mathbf{r}_k , and the two neighboring points \mathbf{r}_{k-1} and \mathbf{r}_{k+1} provided that $\|\mathbf{r}_k - \mathbf{r}_i\| \leq r_w$. If indeed $\|\mathbf{r}_k - \mathbf{r}_i\| \leq r_w$, then $\mathcal{B}_i = \{\mathbf{r}_{k-1}, \mathbf{r}_k, \mathbf{r}_{k+1}\}$, otherwise $\mathcal{B}_i = \emptyset$. We assume that the repulsive force exerted by boundary point $j \in \mathcal{B}_i$ on pedestrian i is given by:

$$\mathbf{f}_{ij}^{bou} = -m_i k_{ij} \frac{(\mu_w \bar{v}_i + v_i^n)^2}{d_{ij}^{bou}} \mathbf{e}_{ij}, \quad (9)$$

where k_{ij} is defined in (8), v_i^n is the component of the velocity normal to the boundary and

$$d_{ij}^{bou} = \|\mathbf{r}_{ij}\| - \frac{1}{2} d_i(\mathbf{v}_i).$$

The complete mathematical model is given by (1), (2), (3), (6), (9).

2.1 Numerical Method

We introduce the time-discretization step $\Delta t > 0$ and set $t^n = n\Delta t$, for $n = 1, \dots, N_t$, with $N_t = T/\Delta t$. Moreover, we denote by y^n the approximation of a generic quantity y at the time t^n .

Each pedestrian i , with $i = 1, \dots, N$, is assigned an initial position \mathbf{r}_i^0 and an initial velocity \mathbf{v}_i^0 . The position at time t^{n+1} , with $n \geq 0$ is found with the following centered finite difference approximation of eq. (1):

$$m_i \frac{\mathbf{r}_i^{n+1} - 2\mathbf{r}_i^n + \mathbf{r}_i^{n-1}}{\Delta t^2} = \mathbf{f}_i^n, \quad n = 0, \dots, N_t - 1, i = 1, \dots, N, \quad (10)$$

where \mathbf{f}_i^n is an approximation of \mathbf{f}_i in eq. (2) at time t^n . Notice that for $n = 0$ in eq. (10) we need \mathbf{r}_i^{-1} , which is computed as follows:

$$\mathbf{r}_i^{-1} = \mathbf{r}_i^0 - \Delta t \mathbf{v}_i^0, \quad i = 1, \dots, N.$$

The velocity of each pedestrian at time t^{n+1} is computed by:

$$\mathbf{v}_i^{n+1} = \frac{\mathbf{r}_i^{n+1} - \mathbf{r}_i^n}{\Delta t}, \quad i = 1, \dots, N. \quad (11)$$

The results presented in Sec. subsec:Calibration, 2.3 and 3 have been obtained with an implementation of the above scheme in MATLAB [36]. The simulations runs on a shared 40-core computing server with 512 GB RAM.

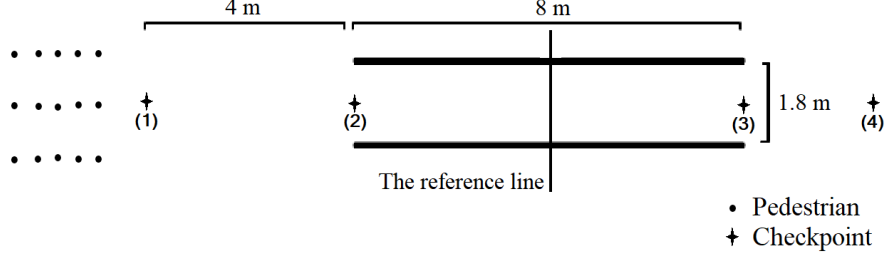


Figure 1: Schematic diagram of the computational domain for the simulations in Sec. 2.2 and 2.3.

2.2 Calibration of the model parameters

The mathematical model described in Sec. 2 depends on several parameters. To understand the model sensitivity to these parameters, we consider the following test. Let Ω be an 8 m long and 1.8 m wide corridor. Initially, the pedestrians are placed as shown in Fig. 1: 4 m from the corridor entrance and 1 m apart from each other. People are initially at rest, i.e. $\mathbf{v}_i^0 = \mathbf{0}$ for $i = 1, \dots, N$. Every pedestrian is assigned the same path: checkpoint 1 to 4, and the radius associated with each of these checkpoints is the corridor width. The desired speed of all pedestrians are Gaussian distributed with mean 1.55 m/s and standard deviation 0.18 m/s [54].

When the simulation is run with the parameters set according to [15] (i.e., $\tau = 0.5$ s, $\tau_d = 0.53$ s, $r_p = r_w = 2$ m, $d_i^0 = 0.18$ m, and $\mu = \mu_w = 0.2$), some pedestrians attain a speed greater than their desired speed. That case makes force (3) change sign and consequently such pedestrians move in the direction opposite to their destination. Furthermore, pedestrian-pedestrian and pedestrian-wall overlaps occur for a large amount of the time interval under consideration. Thus, the parameter values in [15] are suitable for unidirectional motion in a narrow corridor.

The sensitivity analysis for the model parameters τ_d , τ and d_i^0 has been analyzed in detail in [43]. Based on the results therein, we set $\tau_d = 0.20$ s, $\tau = 0.50$ s, $d_i^0 = 0.18$ m and $\Delta t = 0.01$ s from now onwards. Here, we just present the calibration of the cutoff radii r_p and r_w and interaction constant μ in (6) and μ_w in (9) using the aforementioned test.

Let us start with r_p and r_w . Following [15], we set $\mu = \mu_w = 0.2$ for the moment. We take a group of $N = 12$ people and simulate their passage through the corridor. The reason why we choose a small crowd is because in a large group of pedestrians the interaction forces become dominant and it is hard to understand the role of other model parameters. The simulation is run for $T = 13$ s, which is the time it takes all the pedestrians to exit the corridor. We take all the combinations of values for r_p and r_w reported in Table 1. We consider a simulation unstable if the speed of one pedestrian exceeds their desired speed or overlaps (of people) and oscillations (of trajectories) occur. From Table 1, we see that if either of the radii is small, i.e. 1 m, the system is unstable. Among the stable combinations, from now on we consider $r_p = r_w = 2$ m because it the cheapest

	$r_p = 1$ m	$r_p = 2$ m	$r_p = 3$ m
$r_w = 1$ m	unstable	unstable	unstable
$r_w = 2$ m	unstable	stable	stable
$r_w = 3$ m	unstable	stable	stable

Table 1: Stability results for different cutoff radii r_p and r_w values.

computationally.

Next, let us consider the interaction constants in repulsive forces μ in (6) and μ_w in (9). For simplicity, we consider $\mu = \mu_w$. We note that large values of μ help avoid overlaps between pedestrians i and j . On the other hand, when v_{ij} is large and d_{ij} is small, a large value of μ may give rise to a strong repulsive force that compels a pedestrian to deviate more than 90 degrees away from the target direction, leading oscillations in their trajectory. Our goal is to find a value for μ that is large enough to avoid overlaps and small enough to avoid oscillations. For this purpose, we increase the number of pedestrians to $N = 36$. For different values of $\mu = 0, 0.1, 0.2, 0.3, 0.4, 0.5, 0.6$, we run 100 simulations and compute overlap and oscillation quantities defined below.

Following [15], we define

$$O_v = \frac{1}{n_{ov}} \sum_{t=0}^{t=T} \sum_{i=1}^{i=N} \sum_{j>i}^{j=N} o_{ij}, \quad \text{with } o_{ij} = \frac{A_{ij}}{\min(A_i, A_j)} \leq 1, \quad (12)$$

where o_{ij} quantifies the “overlap-strength” and n_{ov} is the cardinality of the set $\{o_{ij} : o_{ij} \neq 0\}$. A_i and A_j are the areas of the discs of pedestrians i and j , and A_{ij} is their area of intersection. If $n_{ov} = 0$, i.e. no overlap occurs, then O_v is set to 0. Notice that the maximum value of O_v is 1.

The oscillation-proportion of a simulation is defined as

$$O_s = \frac{1}{n_{os}} \sum_{t=0}^{t=T} \sum_{i=1}^{i=N} S_i, \quad \text{with } S_i = \frac{1}{2}(-s_i + |s_i|) \quad \text{and } s_i = \frac{v_i \cdot (\overline{v_i} e_i)}{\overline{v_i}^2}, \quad (13)$$

where n_{os} is the cardinality of the set $\{S_i : S_i \neq 0\}$. S_i can be viewed as “oscillation-strength” of pedestrian i . If $n_{os} = 0$, i.e. no oscillation occurs, then O_s is set to 0. Similarly to O_v , the maximum value for O_s is 1.

Fig. 2 shows the average values of O_v and O_s for 100 simulations against μ . We note that for $\mu = 0, 0.1$ most of the simulation are unstable (the speed of some pedestrians exceeded their desired speed). We report the results anyways, although they have little significance. From Fig. 2, we see that O_v decreases as μ , as expected. Aside from the critical values $\mu = 0, 0.1$, O_s increases as μ increases, as expected. The ideal choice appears to be $\mu = \mu_w = 0.3$, which yields no overlap and no oscillations. However, we consider $\mu = \mu_w = 0.2$ an acceptable choice too. Since pedestrians are modeled as discs with a radius that varies with the pedestrian’s speed, we can assume that a

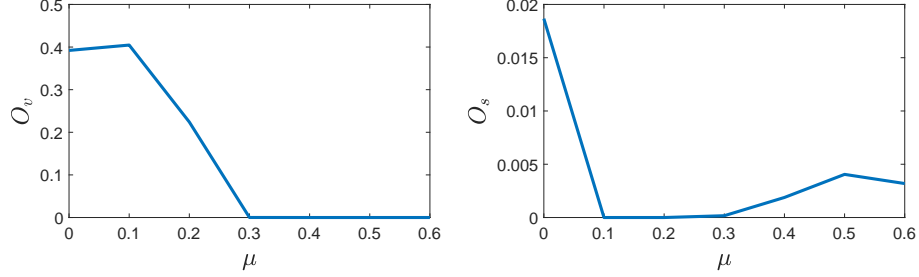


Figure 2: O_v (12) and O_s (13) against the interaction constant μ .

pedestrian does not physically occupy the entire disc. Thus, depending on the test we allow some amount of overlaps in the system.

2.3 Validation Against Experimental Data

We *quantitatively* validate described in model Sec. 2, with the parameters set as explained in Sec. 2.2, by comparing with empirical data from [54]. The experiment geometry is the same as in Fig. 1. A perpendicular line passing through the corridor midline is taken as a reference line. Every pedestrian is assigned the same path: checkpoints 1 to 4. Checkpoint 2 and 4 each have a radius of 1.8 m (width of the corridor), denoted by b_{cor} . Checkpoint 1 has radius b_{ent} and checkpoint 3 has radius b_{exit} . N pedestrians are placed at a distance of 4.5 m from the corridor entrance. The values of b_{ent} , b_{exit} , and N varies for the different experiments. See Table 2.

Experiment Index	N	b_{ent} [m]	b_{exit} [m]
1	60	0.50	1.80
2	66	0.60	1.80
3	111	0.70	1.80
4	121	1.00	1.80
5	175	1.45	1.80
6	220	1.80	1.80
7	170	1.80	1.20
8	160	1.80	0.95
9	148	1.80	0.70

Table 2: Number of people N , entrance width b_{ent} , and exit width b_{exit} for the 9 experiments under consideration.

Over a time interval of length $\delta t = 10$ s, the macroscopic quantities flux $J_{\delta t}$, average velocity

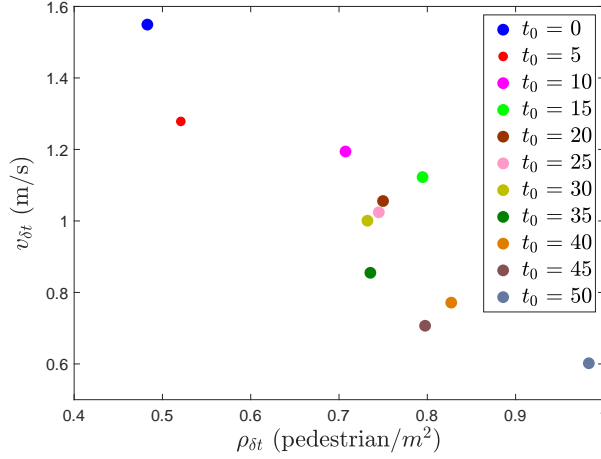


Figure 3: Experiment 1 in Table 2: average velocity $v_{\delta t}$ (14) plotted against density $\rho_{\delta t}$ (14) computed using different values of the initial time for interval δt .

$v_{\delta t}$ and density $\rho_{\delta t}$ are calculated as follows:

$$J_{\delta t} = \frac{N_{\delta t}}{t_{N_{\delta t}}}, \quad v_{\delta t} = \frac{1}{N_{\delta t}} \sum_{i=1}^{i=N_{\delta t}} v_i, \quad \rho_{\delta t} = \frac{J_{\delta t}}{v_{\delta t} b_{cor}}. \quad (14)$$

where $N_{\delta t}$ is the total number of people who crossed the reference line during δt , $t_{N_{\delta t}}$ is the time taken by these $N_{\delta t}$ pedestrians to cross the reference line, and v_i is the velocity of the i^{th} pedestrian at the time they cross the reference line. For every experiment, we will compare the computed and measured quantities defined in (14).

Let $\delta t = [t_0, t_0 + \delta t]$. To decide which t_0 to pick, we consider experiment 1 in Table 2. Fig. 3 shows the computed average velocity plotted against density for different t_0 . We see that when t_0 is in $[10, 30]$ s, the density values are close to each other. Thus, we set $t_0 = 10$ s for experiment 1. The values of t_0 for all the other experiments in Table 2 are set in a similar manner. Then, the densities and average velocities are averaged over 6 runs per experiment.

Fig. 4 shows the computed and measured (from [54]) fundamental diagram for each experiment in Table 2. We observe good agreement: the overall trend is similar, although for certain experiments the computed average velocity for a given density is slightly smaller than the corresponding measured quantity. We remark that the parameters in our model were set as explained in Sec. 2.2 and not tuned to fit the measured data. Thus, some slight difference is to be expected.

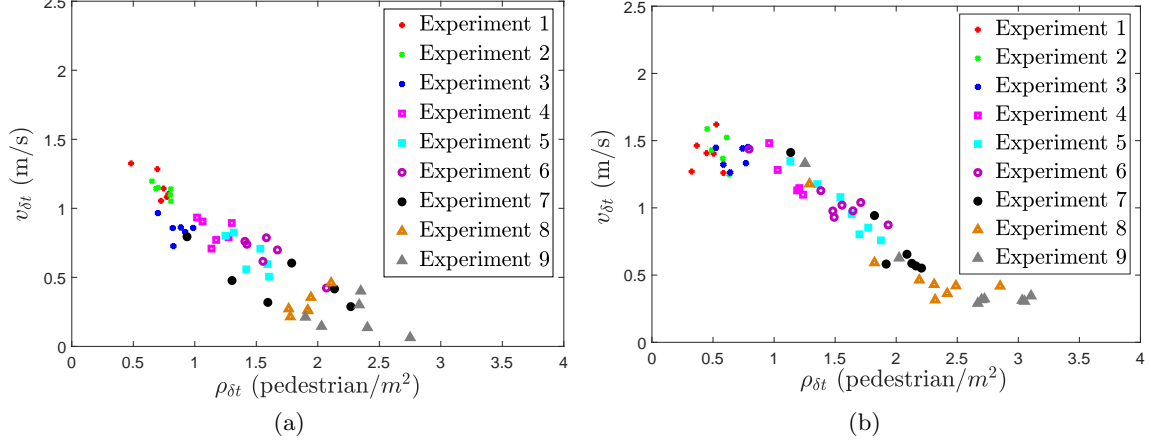


Figure 4: (a) Computed and (b) measured fundamental plots for the 9 experiments in Table 2. The measured data are taken from [54].

3 Bidirectional flow

The experimental validation of our model in Sec. 2.3 involves unidirectional flow of pedestrians. In this section, we consider bidirectional flow. It is known that when groups of people approach each other from opposite directions, they form lanes (see, e.g., [22, 21, 53]), which increase the flow efficiency. We aim at checking that our model, calibrated as reported in Sec. 2.2, can reproduce this spontaneous crowd behavior.

We consider a 20 m long and 5 m wide corridor. Two groups of equal size are initially placed at opposite corridor ends, moving towards each other. Since lane emergence is not immediate, we simulate a periodic corridor. We vary the pedestrian density inside the corridor from 0.2 to 1.6 pedestrians/m², with increment $\Delta\rho = 0.2$ pedestrians/m². Higher values of ρ were not considered as they led to an unstable system in such a small geometry. Recall that for unidirectional flow we could simulate up to $\rho = 2.75$ pedestrians/m² without instabilities (see Fig. 4). So, bidirectional flow in a confined environment seems to be challenging for our model. The number of pedestrians N for each experiment is calculated by $N = \rho * A_c$, where with $A_c = 100$ m² is the corridor area. For all the simulation, every pedestrian has a desired speed of 1 m/s. We remark that pedestrians cannot be initially placed in a symmetric configuration in order to avoid a “frozen state”. See Fig. 5. We let each simulation run until the lane configuration remains stable for 1 minute.

Table. 3 reports the number of lanes formed in each experiments. We observe that for $\rho \leq 1.2$ two lanes form, while for $\rho = 1.4, 1.6$ four lanes form. Fig. 6 show the lane configuration for $\rho = 1$ and 1.4. In Fig. 6 (b) we see that the row of pedestrians near the wall tend to get closer to

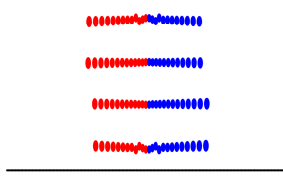


Figure 5: The “frozen state” of a group of 100 pedestrians initially positioned in a symmetric configuration. Red (resp., blue) pedestrians move from left to right (resp., from right to left).

Density (ρ)	0.2	0.4	0.6	0.8	1.0	1.2	1.4	1.6
Number of pedestrians (N)	20	40	60	80	100	120	140	160
Number of lanes	2	2	2	2	2	2	4	4

Table 3: The number of lanes formed in each of the 8 experiments that vary by density ρ and hence by number of pedestrians N .

the wall when they encounter the opposing stream of pedestrians. This is due to the fact that the repulsive force from pedestrians (6) is higher than the repulsive force from the walls (9). When we considered $\rho = 1.8$, we observed two lanes before the system became unstable. See Fig. 7. Notice that we used a different initial configuration than in the $\rho = 1.4$ case in the effort to obtain a stable system. This suggests that the number of lanes for a short period of time is influenced not only by the crowd size but also by the initial positioning.

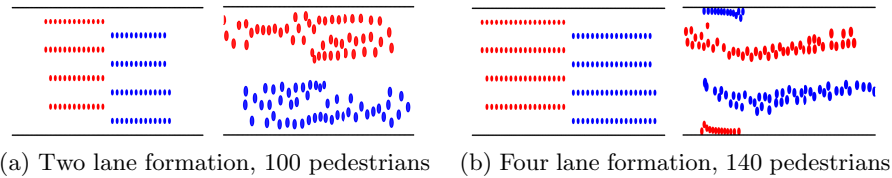


Figure 6: Initial position (left in both panels) and final lane formation configuration (right in both panel) for (a) 100 people and (b) 140 people. Red (resp., blue) pedestrians move from left to right (resp., from right to left).

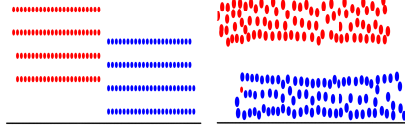


Figure 7: Initial position (left) and lane formation configuration (right) for 180 people before the system becomes unstable. Red (resp., blue) pedestrians move from left to right (resp., from right to left).

4 Simulation of airborne disease spreading using pedestrian dynamics

With the goal of studying the onset of an airborne disease spreading in a complex, yet confined environment we extend the model presented in Sec. 2 by introducing a simple method to trace contact. Depending on the nature of the disease, the sufficient contact time to infect a susceptible person varies. We will focus on a highly infectious disease, like measles.

4.1 A simple model for the spreading of a highly infectious disease

Let us consider a group of N pedestrians in a geometry Ω . Pedestrians can be: sick (infectious), immune (non-susceptible), vulnerable (susceptible), infected and not infected. We define the set of the susceptible and infectious people:

$$\begin{aligned}\mathcal{S} &= \{i \in \mathbb{N}, i \leq N : i^{th} \text{ pedestrian is susceptible}\}, \\ \mathcal{I} &= \{i \in \mathbb{N}, i \leq N : i^{th} \text{ pedestrian is infectious}\},\end{aligned}$$

respectively. In each simulation, P_{imm} % of the population is immune and only a small number of people are sick. The rest of the population is vulnerable.

For a sick person i with position \mathbf{r}_i , we define the set of all susceptible pedestrians that lie inside its circle of influence (sickness domain) at a certain time $t \in (0, T]$ as:

$$\mathcal{I}_i^{sus} = \{j \in \mathcal{S} : \|\mathbf{r}_j - \mathbf{r}_i\| \leq r_s\}, \quad i \in \mathcal{I},$$

where $\|\cdot\|$ denotes the Euclidean norm in \mathbb{R}^2 and r_s is the cutoff radius for the circle of influence. If a pedestrian j stays in \mathcal{I}_i^{sus} for a continuous period of time, e.g. t_v minutes, then they have a v_s % probability of getting infected. After t_v minutes, pedestrian j is moved to either one of the following sets according to its updated stage:

$$\begin{aligned}\mathcal{E}_{sick} &= \{j \in \mathbb{N}, : j \in \mathcal{I}_i^{sus} \text{ for } t_v \text{ mins and is infected}\}, \\ \mathcal{E}_{safe} &= \{j \in \mathbb{N}, : j \in \mathcal{I}_i^{sus} \text{ for } t_v \text{ mins and is not infected}\}.\end{aligned}$$

Once a vulnerable pedestrian moves to either of these sets, they are no longer considered to be in the population that could get infected by sick people, i.e.,

$$\mathcal{S} \cap \mathcal{E}_{sick} = \mathcal{S} \cap \mathcal{E}_{safe} = \emptyset.$$

We also assume that pedestrians belonging to \mathcal{E}_{sick} are not able to transmit the disease, although infected. At the end of each simulation, we will have the number of secondary contacts for the simulated scenario.

In order to simulate the disease spreading in airport terminals, we implemented the pedestrian dynamics model in Sec. 2 and the above contact tracing method in C++. All the simulations ran on a shared 40-core computing server with 512 GB RAM.

4.2 Numerical Results

We consider terminals in two US airports, Hobby Airport in Houston and the Atlanta International Airport, as concrete settings to test our pedestrian dynamics model with contact tracing. We will examine different scenarios: variable population size, variable percentage of immune (non-susceptible) population, boarding bridges or boarding buses. Through the numerical simulations, we quantify the increase in average number of secondary contacts increases as a given terminal becomes more densely populated, the percentage of immune people decreases, the number of primary contacts increases, and areas of high density (such as the boarding buses) are present.

Since we deal with more complicated geometries than the ones tested in Sec. 2 and 3, we handle the checkpoint assignment in a different way. The list of checkpoints contains, for a given checkpoint i , the checkpoint position and a radius r_i . If checkpoint i is in a person's path, the position of the checkpoint for that particular person is randomly picked to be a point inside the circle of radius r_i centered at checkpoint i 's position. This makes each pedestrian's checkpoints unique (if truly random). In addition, this way to assign checkpoints helps to avoid oscillations in pedestrian motion due to clustering of pedestrians around checkpoints that have wait times.

4.3 Hobby Airport in Houston

We consider a part of Houston's William P. Hobby (HOU) Airport as a sample geometry Ω . See Fig. 8. At the start, each of the N pedestrian in Ω is randomly categorized to be either sick, immune or vulnerable. Pedestrians are assigned a random path to pass through the airport. Some people deplane, enter the airport through the terminal gate and leave the airport via the *exit* corridor. Others enter the airport through the *entry* corridor and walk to their assigned terminal gate. Random people are selected to use the restrooms or stop at a restaurant. Departing people are also assigned to randomly check display monitors. Appropriate wait times are allocated for each checkpoint that denotes a restroom, restaurant or a display monitor. Finally, if a person reaches the gate before their boarding time, they stay in the *wait area* near their assigned gate until it is time to board.

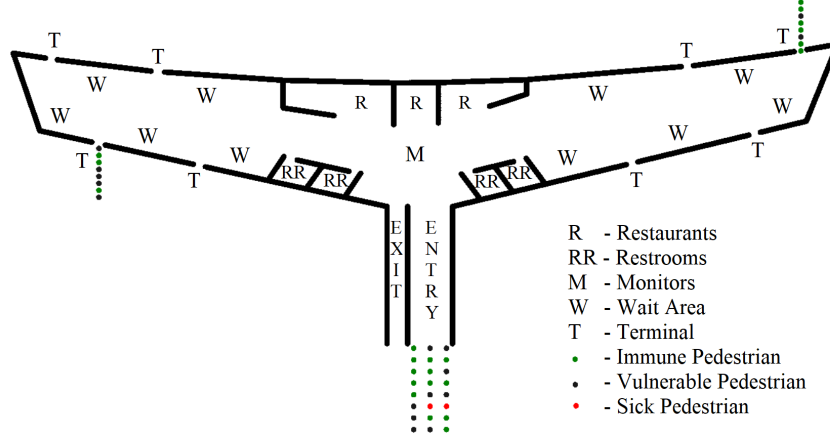


Figure 8: Part of the William P. Hobby Airport in Houston (USA). Pedestrians are represented with a dot.

The pedestrian dynamics model parameters are set as follows: $dt = 0.01$ s, $\tau = 0.5$ s, $\tau_d = 0.18$ s, $r_p = r_w = 2$ m, $d_i^0 = 0.20$ m, and $\mu = \mu_w = 0.3$. For the contact tracing, we set $r_s = 2.5$ m and $v_s = 90\%$. The latter is a realistic value for a highly infectious disease. P_{imm} will vary from 90% to 55% with $\Delta P_{imm} = -5\%$. Remark that herd immunity for a highly infectious disease, like measles, is over 90%. For each P_{imm} , 200 simulations are run to calculate the average number of secondary contacts, which is denoted by Avg_{sc} .

We will consider a simple case to test our implementation (case 1) and a more realistic case (case 2):

- **Case 1:** $N = 400$, $T = 15$ minutes, $t_v = 1$ minute.
- **Case 2:** $N = 1000$, $T = 60$ minutes, $t_v = 2$ minutes.

For each case, we consider two scenarios: a) 1 primary contact and b) 2 primary contacts. We remark that both cases feature a low pedestrian density, given the size of the domain. As expected, our model can handle them efficiently.

Fig. 9 shows two snapshots of a simulation for case 1b. Dots denote people and the color refers to their characterization: red for sick (primary contact), green for immune, black for vulnerable, cyan for infected (secondary contact), and orange for not infected. In Fig. 9 (top), people are deplaning from the rightmost gate while people at the leftmost gate are waiting to deplane. In Fig. 9 (bottom), we see that the primary contact infected several surrounding people in the waiting area.

Fig. 10 shows the average number of secondary contacts for varying P_{imm} . We note that with the exception of $P_{imm} = 75\%$ for case 1, when P_{imm} decreases the number of secondary contacts

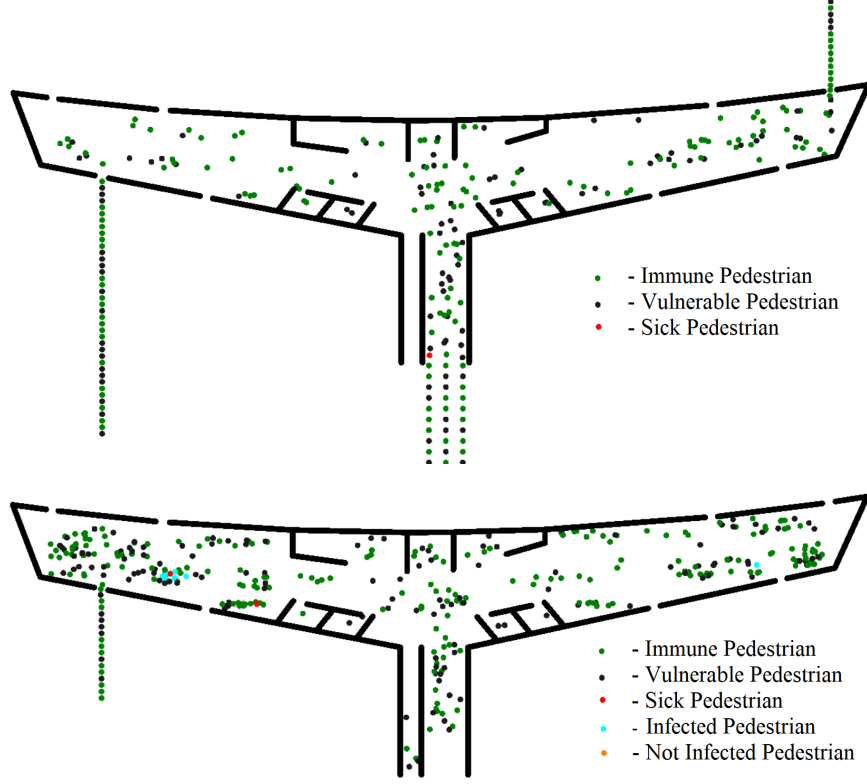


Figure 9: HOU, case 1b: people distribution and characterization after 5 minutes from the start (top) and at the end of the simulation (bottom), i.e. after 12 minutes.

increases for both cases. We also note that Avg_{sc} for case 1 increases slowly as P_{imm} decreases, while the rate of increase of Avg_{sc} is faster for case 2.

Table 4 reports the computed average number of secondary contacts Avg_{sc} , standard deviation Sd_{sc} for all 200 simulations and maximum number of secondary contacts Max_{sc} among all the simulations for cases 1a and 2b, respectively. We see that as P_{imm} decreases, the standard deviation of the number of secondary contacts increases, indicating a wider range of values for the number of secondary contacts. This is reinforced by Fig. 11, where we compare the frequency distributions for cases 1a and 2b. The curves for larger P_{imm} values have taller, narrower peaks as opposed to the curves for smaller P_{imm} values. From Fig. 11 (a) we see that the mode of every distribution is zero, while the mode of every distribution in Fig. 11 (b) is different from zero.

Although at HOU airport passengers board through a boarding bridge, we extend the geometry in Fig. 8 to include buses to transport passengers from the gate to the plane. This is to compare

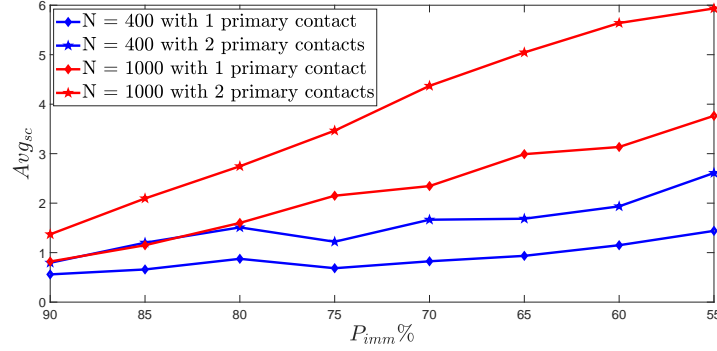


Figure 10: HOU: average number of secondary contacts Avg_{sc} as the population size N and the percentage of immune pedestrians P_{imm} varies.

Case 1a								
$P_{imm} \%$	90	85	80	75	70	65	60	55
Avg_{sc}	0.56	0.66	0.88	0.69	0.83	0.94	1.15	1.44
Sd_{sc}	0.93	0.85	0.99	1.19	1.19	1.12	1.31	1.53
Max_{sc}	4	4	4	7	7	6	7	9
Case 2b								
$P_{immune} \%$	90	85	80	75	70	65	60	55
Avg_{sc}	1.37	2.10	2.75	3.47	4.37	5.05	5.64	5.94
Sd_{sc}	1.30	1.66	2.04	2.53	2.69	2.80	3.37	3.57
Max_{sc}	6	7	10	17	15	15	16	16

Table 4: HOU, case 1a and 2b: computed average number of secondary contacts Avg_{sc} , standard deviation Sd_{sc} for all 200 simulations and maximum number of secondary contacts Max_{sc} among all the simulations.

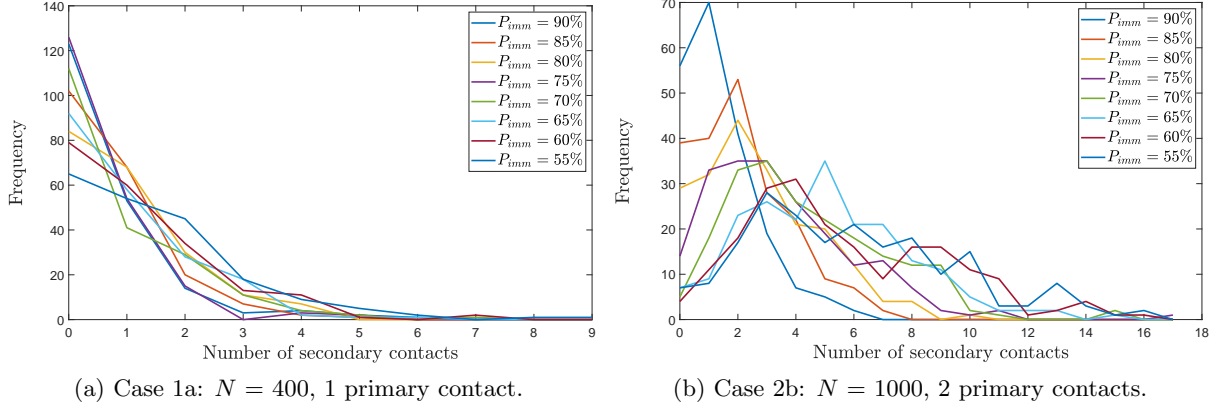


Figure 11: HOU: frequency distribution of the number of secondary contacts produced in 200 simulations for (a) case 1a and (b) case 2b for varying P_{imm} .

the disease spreading in an airport with and without buses. Every departing pedestrian will have their final checkpoint as a random position inside a bus. The pedestrians stay in the bus for 5 minutes and then they board the plane. A bus is 5 m x 12 m and can accommodate 50 people. Fig. 12 shows a screenshot of a simulation in HOU Airport with buses.

We run 200 simulations, with the parameters set as in the case of no buses, in order to calculate Avg_{sc} for $P_{imm} = 90\%$, 80% , 70% , 60% . Fig. 13 shows Avg_{sc} produced in HOU Airport with and without buses. The data in Fig. 13 (a) is the same as in Fig. 10, but with a different scale to facilitate the comparison with Fig. 13 (b). We see that having a high density area such as a bus in the path of pedestrians drastically increases the rate at which people get infected, for a given value of P_{imm} . In addition, the rate at which Avg_{sc} increases as P_{imm} decreases is faster in the airport with buses. We report in Fig. 14 the average number of secondary contacts generated inside the bus. We observe that the cases with the same number of primary contacts have average values closer to each other. The population size N makes less of a difference because the number of people in the buses does not change significantly between case 1 and 2.

Finally, to estimate the basic reproduction number, we set $P_{imm} = 0\%$ for cases 1a and 2a. Table 5 reports the basic reproduction number averaged over 200 simulations for both cases without and with buses. For both cases, the buses contribute to an increase of roughly 5 infected people.

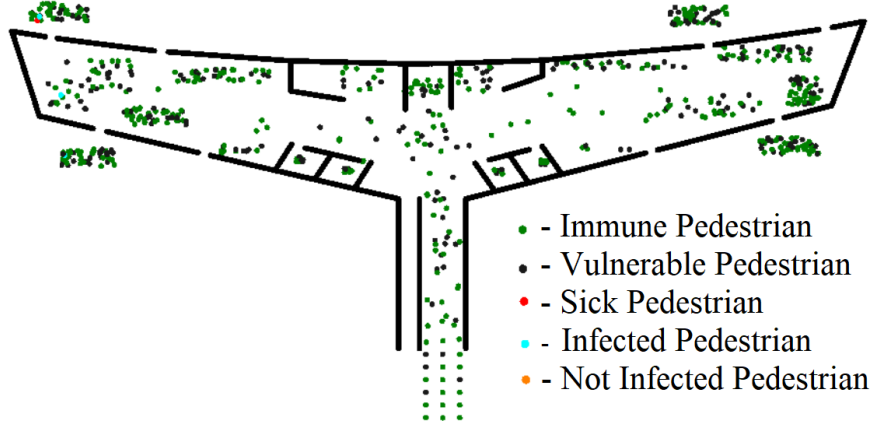


Figure 12: HOU with buses: screenshot of a simulation. Pedestrians are represented with a dot and color encodes the different characterization.

	Without Buses	With Buses
case 1a	2.4	7.66
case 2a	9.305	15.21

Table 5: HOU: average basic reproduction number without and with buses.

4.4 Connecting airports: Hobby Airport to Atlanta International Airport

The set of tests presented in this section involves one or two primary contacts that takes a flight from Hobby Airport (shown in Fig. 8) to Hartsfield-Jackson Atlanta International (ATL) Airport. We will only consider the part of ATL airport shown in Fig. 15. In all the simulations, the primary contact(s) enters HOU airport through security check, moves through the terminal to reach the gate of their flight, boards the plane to ATL airport. Once at ATL airport, the primary contact(s) moves through the terminal to reach the gate of their final flight. Just like for the results in Sec. 4.3, some people enter ATL airport through the entry corridor and board a flight, while others enter through the gates. Ten percent of the latter group goes onto boarding a flight, while the rest leave the airport through the exit. In addition, random people are selected to use the restrooms or stop at a restaurant and departing people are also assigned to randomly check display monitors. We will consider the case of both airports with and without buses.

All the parameters are set like in Sec. 4.3. However, we limit the values of P_{imm} to 90%, 80%, 70%, 60% and we consider only one case: $N = 1000$, $T = 50$ minutes, $t_v = 2$ minutes, with a) 1 primary contact and b) 2 primary contacts. For each scenario, we run 200 simulations and calculate the average number of secondary contacts Avg_{sc} .

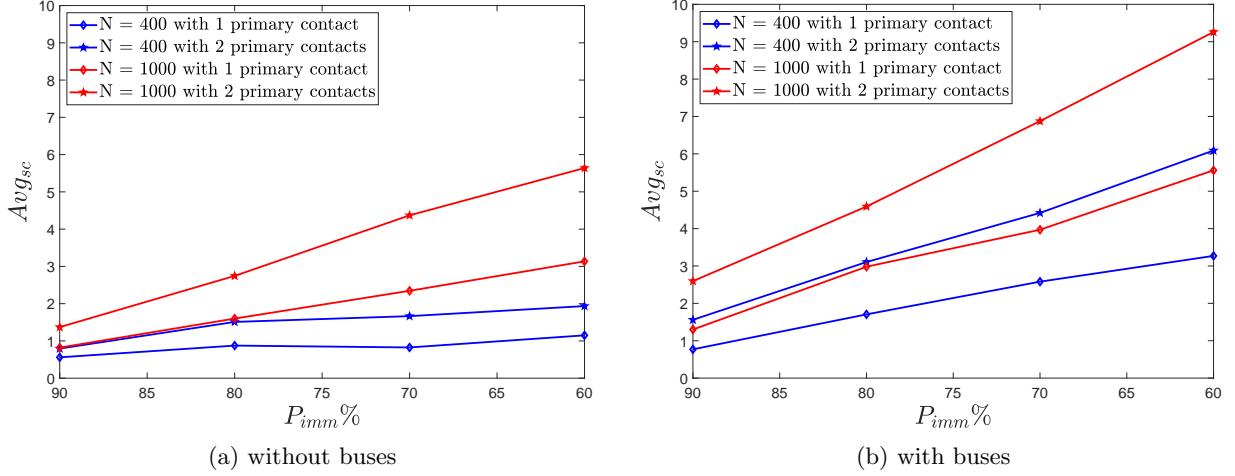


Figure 13: HOU: average number of secondary contacts Avg_{sc} produced (a) without buses and (b) with buses as the percentage of immune pedestrians P_{imm} varies.

To simplify the simulation, the sick person can infect vulnerable people only inside the terminals and, if present, in the buses. In this way, the simulations in each airport can be run in parallel. Fig. 16 (a) shows the initial people distribution for one of the simulations in ATL airport with the buses. The pedestrians inside the buses spend 5 minutes there before they reach the terminal. The people in the terminal are waiting to board their planes. The rest of the pedestrians, including the primary contact(s), will enter the airport later as per their assigned arrival time (if deplaning) or 15 minutes into the simulation (if entering through the entry corridor). Fig. 16 (b) shows the people distribution and characterization after 20 minutes.

Fig. 17 reports the the average number of secondary contacts for case 1a and 1b with and without buses. By comparing Fig. 17 (a) and (b), we see that the number of secondary contacts is more than doubled in presence of the buses. These results confirm that: (i) a high percentage of immune pedestrians in the system ensures that the number of infected people remain small and (ii) the spreading of the disease is amplified by the airport buses.

Fig. 18 displays the average number of secondary contacts produced inside the buses vs inside the ATL terminal for cases 1a and 1b. We notice that the average number of people infected by one primary contact inside the buses is close to the average number of people infected by two primary contacts inside the terminal.

Finally, to estimate the basic reproduction number in ATL airport we set $P_{imm} = 0\%$ for case 1a. Table 6 reports the basic reproduction number averaged over 200 simulations for cases 1a

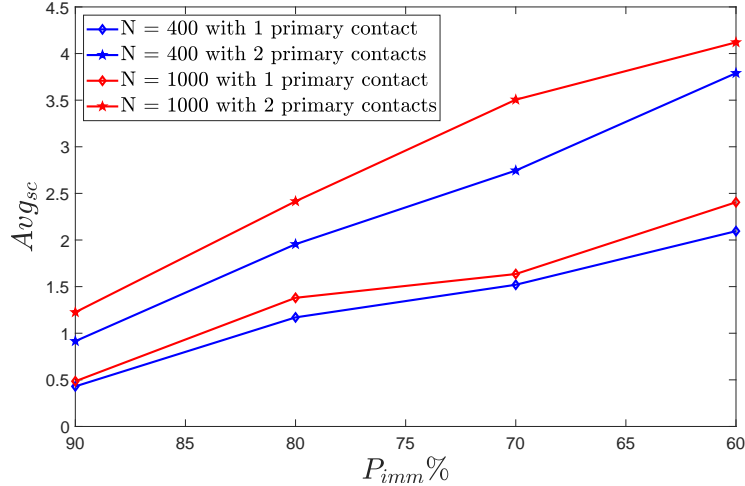


Figure 14: HOU: average number of secondary contacts generated inside the buses as the percentage of immune pedestrians P_{imm} varies.

	Without Buses	With Buses
Case 1a	7.263	18.693

Table 6: Average basic reproduction number in the geometry in Fig. 15 without and with buses.

without and with buses.

5 Conclusions

We combined a grid free, force-based microscopic model for pedestrian dynamics with a contact tracing method to study the initial spreading of a highly infectious airborne disease in a confined environment. The pedestrian dynamics model is calibrated to avoid unrealistic pedestrian motion (overlap of people and oscillating walking trajectories) and validated against empirical data from [54]. In addition, we showed that lane formation in bidirectional flow (a well known self organizing phenomenon) is captured by the pedestrian dynamics model under consideration. The contact tracing method uses a sickness domain around each sick person. A susceptible person has a prescribed probability to become infected if they stay in a sickness domain for a certain amount of time.

To test our model of pedestrian dynamics with contact tracing, we considered medium size populations with immune and susceptible people in the terminals of two US airports. We computed the average number of secondary contacts produced by one or two primary contacts in a single terminal or in terminals of different airports connected by a flight hosting a primary contact. We

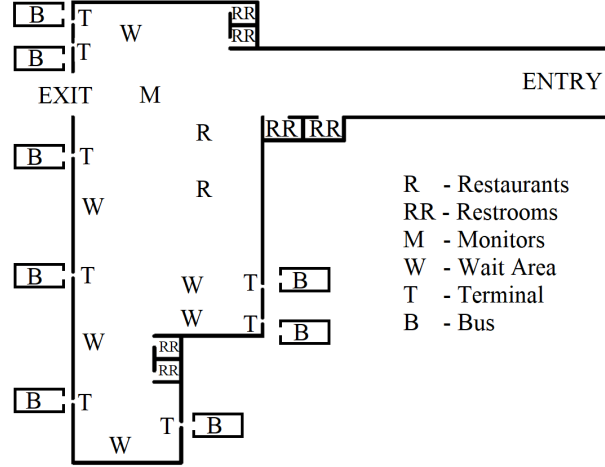


Figure 15: Part of the Hartsfield-Jackson Atlanta International Airport in Atlanta (USA) used for the simulations.

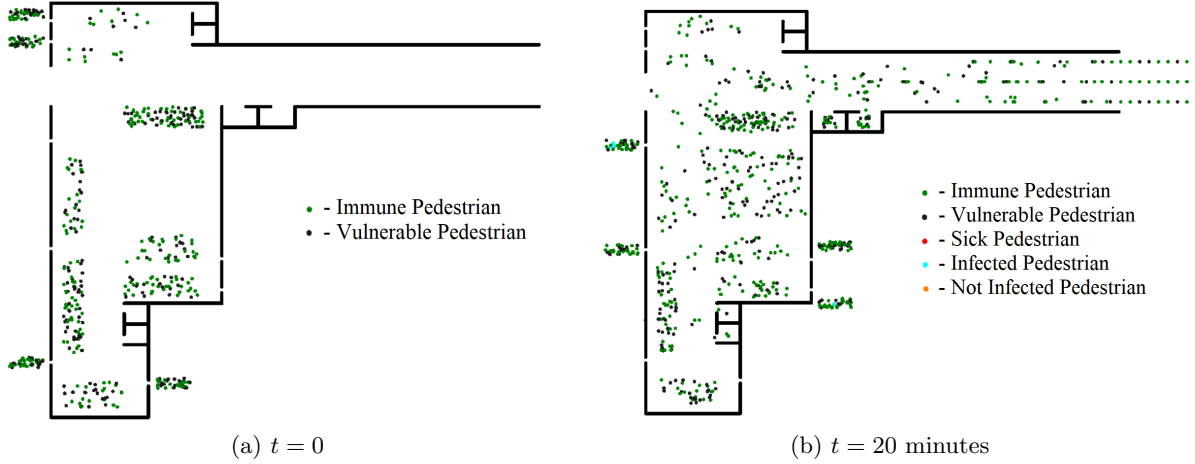


Figure 16: ATL, case 1a: (a) initial people distribution and characterization and (b) after 20 minutes.

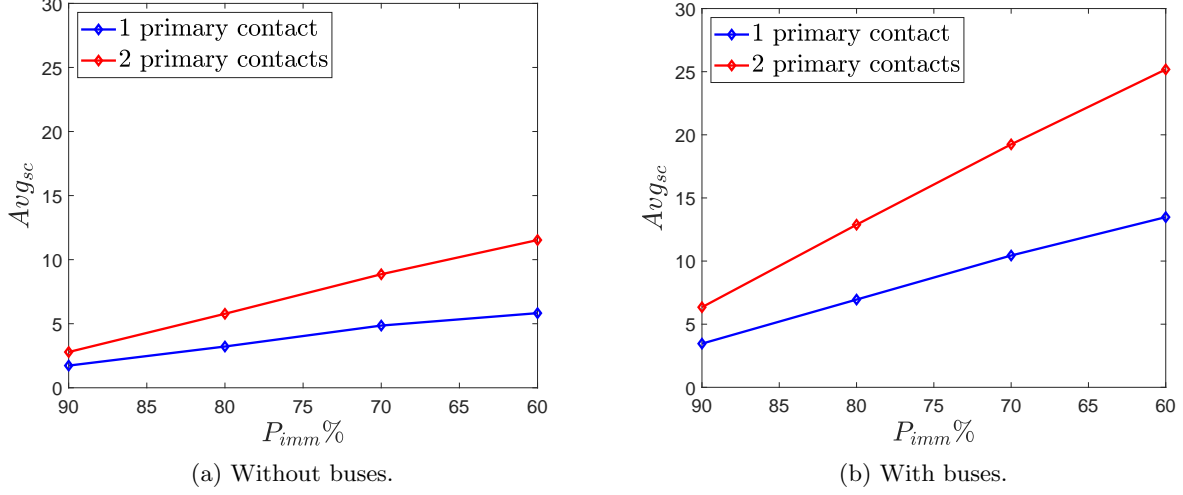


Figure 17: HOU to ATL (a) with buses or (b) without buses: average number of secondary contacts produced by 1 or 2 primary contacts for different values of P_{imm} . Each airport contains 1000 people.

also considered the case where people could board a bus to reach their planes. Sick people were traced only when inside airports or buses. In the case of airports without buses, we concluded that:

- For same size populations, an increase in primary contacts causes an increase in the average number of infected pedestrians that becomes larger as the percentage of immune population decreases.
- The larger the population size, the higher the rate of increase in the average number of infected pedestrians.
- A higher population density leads to an increase in average number of secondary contacts for a fix percentage of immune population.

In the case of airports with buses (high density areas), we showed the drastic increase in the rate at which people are getting infected.

The combination of pedestrian dynamics model with contact tracing method could be used in different settings (emergency rooms, hospitals, etc.) and tailored to airborne diseases with different spreading mechanisms. If further tested and validated, it could become a tool to investigate best practices that can help reduce the spreading of a disease.

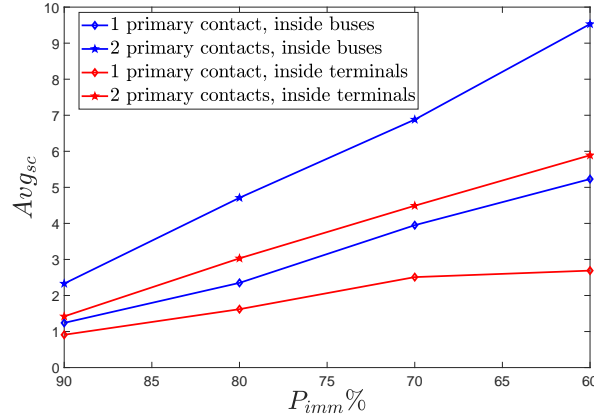


Figure 18: ATL, cases 1a and 1b: average number of secondary contacts produced for different P_{imm} in specific locations (only inside buses vs only inside the terminal).

Acknowledgements

This work has been partially supported by NSF through grant DMS-1620384. We acknowledge fruitful discussions with Drs. Ilya Timofeyev and William Fitzgibbon.

References

- [1] J. P. Agnelli, F. Colasuonno, and D. Knopoff. A kinetic theory approach to the dynamics of crowd evacuation from bounded domains. *Mathematical Models and Methods in Applied Sciences*, 25(01):109–129, 2015.
- [2] Frank G. Ball, Edward S. Knock, and Philip D. O’Neill. Threshold behaviour of emerging epidemics featuring contact tracing. *Advances in Applied Probability*, 43(4):1048–1065, 2011.
- [3] N. Bellomo, D. Knopoff, and J. Soler. On the difficult interplay between life, “complexity”, and mathematical sciences. *Mathematical Models and Methods in Applied Sciences*, 23(10):1861–1913, 2013.
- [4] N. Bellomo, B. Piccoli, and A. Tosin. Modeling crowd dynamics from a complex system viewpoint. *Mathematical Models and Methods in Applied Sciences*, 22(supp02):1230004, 2012.
- [5] Nicola Bellomo and Abdelghani Bellouquid. On the modeling of crowd dynamics: Looking at the beautiful shapes of swarms. *Networks and Heterogeneous Media*, 6(3):383–399, 2011.

- [6] Nicola Bellomo, Abdelghani Bellouquid, Livio Gibelli, and Nisrine Outada. *A quest towards a mathematical theory of living systems*. Modeling and Simulation in Science, Engineering and Technology. Birkhauser, 2017.
- [7] Nicola Bellomo, Abdelghani Bellouquid, and Damian Knopoff. From the microscale to collective crowd dynamics. *SIAM Multiscale Model. Simul.*, 11:943–963, 2013.
- [8] Nicola Bellomo and Christian Dogbe. On the modeling of traffic and crowds: A survey of models, speculations, and perspectives. *SIAM Review*, 53(3):409–463, 2011.
- [9] Nicola Bellomo and Livio Gibelli. Toward a mathematical theory of behavioral-social dynamics for pedestrian crowds. *Math. Models Methods Appl. Sci.*, 25(13):2417–2437, 2015.
- [10] Nicola Bellomo and Livio Gibelli. Behavioral crowds: Modeling and Monte Carlo simulations toward validation. *Computers and Fluids*, 141:13–21, 2016.
- [11] Nicola Bellomo, Livio Gibelli, and Nisrine Outada. On the interplay between behavioral dynamics and social interactions in human crowds. *Kinetic and Related Models*, 12(2):397–409, 2019.
- [12] Glenn Webb Cameron Browne, Hayriye Gulbudak. Modeling contact tracing in outbreaks with application to ebola. *Journal of Theoretical Biology*, 384:33–49, 2015.
- [13] M. Chraibi, A. Seyfried, A. Schadschneider, and W. Mackens. Quantitative description of pedestrian dynamics with a force-based model. In *IEEE/WIC/ACM International Joint Conference on Web Intelligence and Intelligent Agent Technology IEEE Computer Society, Los Alamitos, CA*, volume 3, pages 583–586, 2009.
- [14] Mohcine Chraibi, Ulrich Kemloh, Andreas Schadschneider, and Armin Seyfried. Force-based models of pedestrian dynamics. *Networks and Heterogeneous Media*, 6(3):425–442, 2011.
- [15] Mohcine Chraibi, Armin Seyfried, and Andreas Schadschneider. Generalized centrifugal-force model for pedestrian dynamics. *Phys. Rev. E*, 82:046111, Oct 2010.
- [16] Martin Eichner. Case isolation and contact tracing can prevent the spread of smallpox. *American Journal of Epidemiology*, 158:118128, 2003.
- [17] C Fraser, S Riley, R.M Anderson, and Ferguson N.M. Factors that make an infectious disease outbreak controllable. *Proc. Natl Acad. Sci. USA*, 101:61466151, 2004.
- [18] Anderson R.M Garnett G.P. Sexually transmitted diseases and sexual behavior: insights from mathematical models. *J. Infect. Dis.*, 174:S150S161, 1996.

- [19] Giorgio Guzzetta, Marco Ajelli, Zhenhua Yang, Leonard N. Mukasa, Naveen Patil, Denise E. Kirschner, and Stefano Merler. Effectiveness of contact investigations for tuberculosis control in Arkansas. *Journal of Theoretical Biology*, 380:238246, 2015.
- [20] Dirk Helbing. A mathematical model for the behavior of pedestrians. *Behavioral Science*, 36(4):298–310, 1991.
- [21] Dirk Helbing. Collective phenomena and states in traffic and self-driven many-particle systems. *Computational Materials Science*, 30(12):180 – 187, 2004. Selected papers of the Twelfth International Workshop on Computational Materials Science (CMS2002).
- [22] Dirk Helbing and Péter Molnár. Social force model for pedestrian dynamics. *Phys. Rev. E*, 51:4282–4286, May 1995.
- [23] Dirk Helbing and Tamas Vicsek. Optimal self-organization. *New Journal of Physics*, 1(1):13, 1999.
- [24] Yorke J.A Hethcote H.W. Gonorrhea transmission dynamics and control. *Springer Lecture Notes in Biomathematics, Berlin:Springer*, 1984.
- [25] Roger L. Hughes. A continuum theory for the flow of pedestrians. *Transportation Research Part B: Methodological*, 36(6):507 – 535, 2002.
- [26] James M. Hyman, Jia Li, and E. Ann, Stanley. Modeling the impact of random screening and contact tracing in reducing the spread of HIV. *Mathematical Biosciences*, 181:17–54, 2003.
- [27] Anders Johansson, Dirk Helbing, and Pradyumn K. Shukla. Specification of the social force pedestrian model by evolutionary adjustment to video tracking data. *Advances in Complex Systems*, 10(supp02):271–288, 2007.
- [28] McKendrick A.G Kermack W.O. A contribution to the mathematical theory of epidemics. *Proc. R. Soc.*, 115:700721, 1927.
- [29] Daewa Kim and Annalisa Quaini. A kinetic theory approach to model pedestrian dynamics in bounded domains with obstacles. *Kinetic and Related Models*, 12(6):1273–1296, 2019.
- [30] Istvan Z Kiss, Darren M Green, and Rowland R Kao. Disease contact tracing in random and clustered networks. *Proceedings of the Royal Society B*, 272:14071414, 2005.
- [31] Don Klinkenberg, Christophe Fraser, and Hans Heesterbeek. The effectiveness of contact tracing in emerging epidemics. *PLOS ONE*, 1(1):1–7, 12 2006.
- [32] Taras I. Lakoba, D. J. Kaup, and Neal M. Finkelstein. Modifications of the Helbing-Molnar-Farkas-Vicsek social force model for pedestrian evolution. *SIMULATION*, 81(5):339–352, 2005.

- [33] S. Liu, S. Lo, J. Ma, and W. Wang. An agent-based microscopic pedestrian flow simulation model for pedestrian traffic problems. *IEEE Transactions on Intelligent Transportation Systems*, 15(3):992–1001, June 2014.
- [34] Shaobo Liu, Lizhong Yang, Tingyong Fang, and Jian Li. Evacuation from a classroom considering the occupant density around exits. *Physica A: Statistical Mechanics and its Applications*, 388(9):1921 – 1928, 2009.
- [35] Jian Ma, Wei guo Song, Jun Zhang, Siu ming Lo, and Guang xuan Liao. k-nearest-neighbor interaction induced self-organized pedestrian counter flow. *Physica A: Statistical Mechanics and its Applications*, 389(10):2101 – 2117, 2010.
- [36] MATLAB. <https://www.mathworks.com/products/matlab.htm>.
- [37] Notes from the Field: Measles Transmission at a Domestic Terminal Gate in an International Airport – United States, January 2014. <https://www.cdc.gov/mmwr/preview/mmwrhtml/mm6350a9.htm>.
- [38] Notes from the Field: Measles Transmission in an International Airport at a Domestic Terminal Gate – April-May 2014. <https://www.cdc.gov/mmwr/preview/mmwrhtml/mm6424a6.htm>.
- [39] Mehdi Moussaïd, Dirk Helbing, Simon Garnier, Anders Johansson, Maud Combe, and Guy Theraulaz. Experimental study of the behavioural mechanisms underlying self-organization in human crowds. *Proceedings of the Royal Society of London B: Biological Sciences*, 276(1668):2755–2762, 2009.
- [40] Anuj Mubayi, Christopher Kribs Zaleta, Maia Martcheva, and Carlos Castillo-Chavez. A cost-based comparison of quarantine strategies for new emerging diseases. *Mathematical Biosciences and Engineering*, 7(1551-0018-2010-3-687):687, 2010.
- [41] Johannes Mueller, Mirjam Kretzschmar, and Klaus Dietz. Contact tracing in stochastic and deterministic epidemic models. *Mathematical Biosciences*, 164:39–64, 2000.
- [42] D.R. Parisi and C.O. Dorso. Morphological and dynamical aspects of the room evacuation process. *Physica A: Statistical Mechanics and its Applications*, 385(1):343 – 355, 2007.
- [43] K. Rathinakumar. *A Microscopic Approach to Pedestrian Dynamics and the Onset of Disease Spreading*. PhD thesis, University of Houston, 2019.
- [44] C.M. Rivers, E.T. Lofgren, M. Marathe, S. Eubank, and B.L. Lewis. Modeling the impact of interventions on an epidemic of ebola in Sierra Leone and Liberia. *PLoS Curr.*, 6, 2014.
- [45] P Rohani, D.J.D Earn, and B.T Grenfell. The impact of immunisation on pertussis transmission in england and wales. *Lancet*, 355:285286, 2000.

- [46] Andreas Schadschneider, Wolfram Klingsch, Hubert Klüpfel, Tobias Kretz, Christian Rogsch, and Armin Seyfried. *Evacuation Dynamics: Empirical Results, Modeling and Applications*, pages 517–550. Springer New York, New York, NY, 2011.
- [47] Armin Seyfried, Oliver Passon, Bernhard Steffen, Maik Boltes, Tobias Rupperecht, and Wolfram Klingsch. New insights into pedestrian flow through bottlenecks. *Transportation Science*, 43(3):395–406, 2009.
- [48] A. Shende, M. P. Singh, and P. Kachroo. Optimization-based feedback control for pedestrian evacuation from an exit corridor. *IEEE Transactions on Intelligent Transportation Systems*, 12(4):1167–1176, Dec 2011.
- [49] Yusuke Tajima, Kouhei Takimoto, and Takashi Nagatani. Pattern formation and jamming transition in pedestrian counter flow. *Physica A: Statistical Mechanics and its Applications*, 313(3):709 – 723, 2002.
- [50] Alasdair Turner and Alan Penn. Encoding natural movement as an agent-based system: An investigation into human pedestrian behaviour in the built environment. *Environment and Planning B: Planning and Design*, 29(4):473–490, 2002.
- [51] Jonathan A. Ward, Andrew J. Evans, and Nicolas S. Malleson. Dynamic calibration of agent-based models using data assimilation. *Royal Society Open Science*, 3(4), 2016.
- [52] S. Xu and H. B. L. Duh. A simulation of bonding effects and their impacts on pedestrian dynamics. *IEEE Transactions on Intelligent Transportation Systems*, 11(1):153–161, March 2010.
- [53] W. J. Yu, R. Chen, L. Y. Dong, and S. Q. Dai. Centrifugal force model for pedestrian dynamics. *Phys. Rev. E*, 72:026112, Aug 2005.
- [54] J. Zhang, W. Klingsch, A. Schadschneider, and A. Seyfried. Transitions in pedestrian fundamental diagrams of straight corridors and T-junctions. *J. Stat. Mech.*, 2011:P06004, 2011.
- [55] B. Zhou, X. Wang, and X. Tang. Understanding collective crowd behaviors: Learning a mixture model of dynamic pedestrian-agents. In *2012 IEEE Conference on Computer Vision and Pattern Recognition*, pages 2871–2878, June 2012.